

SuperOcc: Toward Cohesive Temporal Modeling for Superquadric-based Occupancy Prediction

Zichen Yu, Quanli Liu, *Member, IEEE*, Wei Wang, *Senior Member, IEEE*,
Liyong Zhang, *Member, IEEE*, and Xiaoguang Zhao

Abstract—3D occupancy prediction plays a pivotal role in the realm of autonomous driving, as it provides a comprehensive understanding of the driving environment. Most existing methods construct dense scene representations for occupancy prediction, overlooking the inherent sparsity of real-world driving scenes. Recently, 3D superquadric representation has emerged as a promising sparse alternative to dense scene representations due to the strong geometric expressiveness of superquadrics. However, existing superquadric frameworks still suffer from insufficient temporal modeling, a challenging trade-off between query sparsity and geometric expressiveness, and inefficient superquadric-to-voxel splatting. To address these issues, we propose SuperOcc, a novel framework for superquadric-based 3D occupancy prediction. SuperOcc incorporates three key designs: (1) a cohesive temporal modeling mechanism to simultaneously exploit view-centric and object-centric temporal cues; (2) a multi-superquadric decoding strategy to enhance geometric expressiveness without sacrificing query sparsity; and (3) an efficient superquadric-to-voxel splatting scheme to improve computational efficiency. Extensive experiments on the SurroundOcc and Occ3D benchmarks demonstrate that SuperOcc achieves state-of-the-art performance while maintaining superior efficiency. The code is available at <https://github.com/Yzichen/SuperOcc>.

Index Terms—3D occupancy prediction, autonomous driving, temporal modeling, computer vision

I. INTRODUCTION

VISION-CENTRIC 3D scene understanding is a core research direction in autonomous driving. Existing approaches primarily focused on 3D object detection [1]–[5], predicting 3D bounding boxes of traffic participants to provide object-level representations. However, they struggle to handle out-of-vocabulary or arbitrarily shaped objects, which significantly compromises the safety and reliability of driving systems [6], [7]. To overcome this limitation, 3D occupancy prediction divides the scene into voxel grids and jointly predicts the occupancy state and semantic label of each voxel. Compared with 3D object detection, occupancy prediction

Zichen Yu, Quanli Liu, Wei Wang and Liyong Zhang are with the School of Control Science and Engineering, Dalian University of Technology, Dalian 116024, China, and also with the Dalian Rail Transmit Intelligent Control and Intelligent Operation Technology Innovation Center, Dalian 116024, China (e-mail: yuzichen@mail.dlut.edu.cn; liuql@dlut.edu.cn; wangwei@dlut.edu.cn; zhly@dlut.edu.cn).

Xiaoguang Zhao is with the Dalian Rail Transmit Intelligent Control and Intelligent Operation Technology Innovation Center, Dalian 116024, China, and also with the Dalian Seasky Automation Co., Ltd, Dalian 116024, China (e-mail: xiaoguang.zhao@dlssy.com).

This work was supported in part by the National Natural Science Foundation of China under Grant 62373077, in part by the Science and Technology Joint Plan of Liaoning Province under Grant 2024JH2/102600014, in part by the Fundamental Research Funds for the Central Universities under Grant DUTZD25203 and in part by the Key Field Innovation Team Support Plan of Dalian, China, under Grant 2021RT02. (Corresponding author: Quanli Liu).

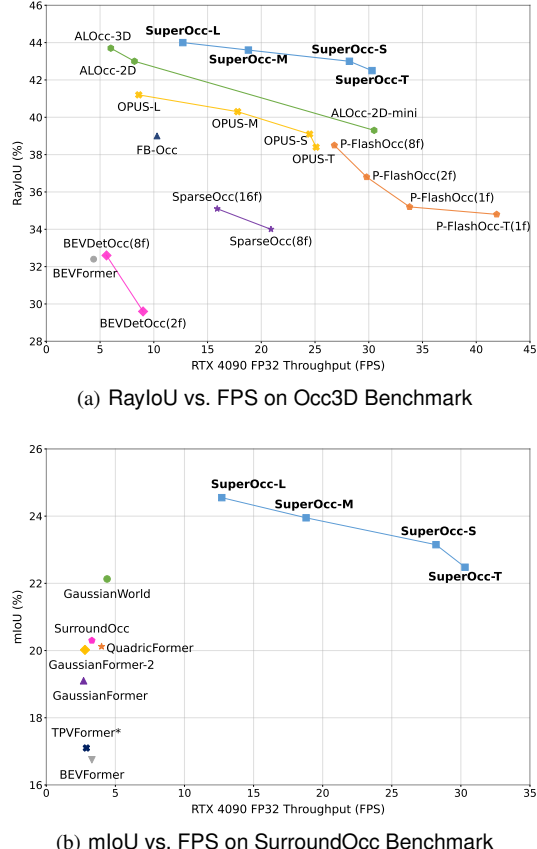


Fig. 1. Comparison of speed-accuracy trade-offs of different methods on (a) Occ3D and (b) SurroundOcc benchmarks. SuperOcc achieves the optimal trade-off, delivering high accuracy while maintaining efficient inference.

offer a unified representation of all scene elements, enabling more comprehensive and fine-grained scene understanding.

3D occupation prediction is essentially a 3D semantic segmentation task. Therefore, early methods [6]–[10] directly generate dense volumetric feature representations followed by per-voxel classification. These methods are intuitive and capable of capturing sufficient geometric details, but they suffer from high computational complexity and memory consumption. To alleviate this burden, subsequent studies have extensively explored alternative dense representations [11]–[13] and more efficient learning schemes [14], [15]. Although these methods effectively reduce computational costs, they still fail to fully exploit the spatial sparsity of real-world scenes, i.e., the vast majority of 3D space is actually free. Consequently, performing uniform computation and prediction across these free regions introduces considerable computa-

tional redundancy and resource waste.

To align with the inherent sparsity of driving scenes, recent research [16]–[21] has begun exploring sparse scene representations. Gaussian-based methods [18], [19] describe scenes sparsely using a set of 3D semantic gaussians, and each of them is responsible for modeling a flexible region of interest. However, the strong elliptical priors limit their ability to model diverse geometric shapes. Superquadric-based methods [21], [22] address this limitation by introducing geometrically expressive superquadrics as scene primitives. With a compact parametric representation, superquadrics can generate a rich variety of geometric shapes, allowing complex structures to be modeled effectively without dense stacking. Despite the significant progress made by superquadric-based methods in scene representation, they still suffer from the following key limitations:

- **Insufficient Temporal Modeling.** Existing temporal-aware methods are restricted to a singular modeling paradigm, i.e., view-centric or object-centric temporal modeling. The former exploits historical image features to provide fine-grained spatio-temporal context, while the latter propagates temporal information via sparse queries focusing on high-level semantic and geometric abstractions. The absence of a unified temporal modeling strategy limits the effective utilization of temporal cues in dynamic scenes.
- **Challenging Trade-off between Query Sparsity and Geometric fidelity.** Current frameworks decode each query into a single superquadric primitive, which severely constrains the geometric expressiveness of individual queries. As a result, it is difficult to accurately reconstruct complex driving scenarios with a limited number of queries, forcing a challenging trade-off between geometric fidelity and query sparsity.
- **Inefficient Superquadric-to-Voxel Splatting.** The implementation of the superquadric-to-voxel splatting lacks operator-level optimization tailored for the CUDA architecture, resulting in redundant memory usage and inefficient computation. This constrains the model’s deployment potential in resource-constrained in-vehicle systems.

To address these limitations, we propose a novel framework SuperOcc for superquadric-based 3D occupancy prediction. It mainly contains three key designs: 1) The **cohesive temporal modeling mechanism** is developed to simultaneously leverage view-centric and object-centric temporal modeling within a unified framework. For the former, we maintain a memory queue to cache historical image features, which are sampled and aggregated to provide fine-grained spatio-temporal context. For the latter, sparse queries serve as hidden states for temporal propagation. Historical queries are stored in a memory queue and propagated to the subsequent frame following temporal alignment. They can provide informative spatial and semantic priors for subsequent predictions, since the evolution of the driving scenarios is continuous. This dual-path integration enables the model to comprehensively exploit temporal cues, improving both the accuracy and stability of occupancy predictions in dynamic driving scenarios. 2) The

multi-superquadric decoding strategy is designed to enhance the model’s geometric expressiveness while preserving query sparsity. Built upon the superquadric-based scene representation, this strategy decodes each query into a local cluster of superquadrics in a coarse-to-fine manner. This allows a single query to model intricate geometric structures with high fidelity. Consequently, complex 3D scenes can be accurately represented even with only a few hundred sparse queries. 3) The **efficient superquadric-to-voxel splatting scheme** is implemented to accelerate the transformation from 3D superquadric representations to 3D semantic occupancy. By introducing a tile-level binning strategy and leveraging GPU shared memory, this optimization substantially reduces computational complexity and memory access overhead, significantly improving both training and inference efficiency.

Overall, our contributions are summarized as follows:

- We propose SuperOcc, a novel 3D occupancy prediction framework that introduces a cohesive temporal modeling mechanism. This mechanism captures fine-grained spatio-temporal context from historical image features and efficiently leverages informative historical priors through query propagation, thereby enhancing occupancy modeling accuracy in dynamic driving scenarios.
- We design a multi-superquadric decoding strategy to boost the geometric expressiveness of sparse queries, alongside an efficient superquadric-to-voxel splatting implementation to significantly reduce training costs and improve inference efficiency.
- We evaluate SuperOcc on the challenging Occ3D [6] and SurroundOcc [9] benchmarks, achieving state-of-the-art (SOTA) performance while maintaining superior efficiency, as illustrated in Fig. 1.

II. RELATED WORKS

A. Camera-based 3D Occupancy Prediction

1) *Dense Scene Representation:* Dense scene representation is the most straightforward modeling paradigm. Existing methods [6], [8]–[10], [14], [15], [23]–[26] typically discretizes the 3D space into voxel grids to construct a dense volume representation. FB-OCC [8] employs depth-aware back-projection to complete and enhance the initial 3D volume generated by forward projection. SurroundOcc [9] adopts a 2D-3D spatial attention mechanism to integrate multi-camera information into 3D volume queries and construct 3D volume features in a multi-scale manner. Although these methods are capable of capturing rich geometric details, they suffer from high computational cost and memory overhead. Subsequent works therefore aim to improve the efficiency of dense volume construction and processing. OccFormer [10] decomposes heavy 3D processing into local and global transformer pathways along the horizontal plane to efficiently process the 3D volume. CTF-Occ [6] introduces an incremental token selection strategy to mitigate the computational burden caused by dense sampling. To better balance performance and efficiency, COTR [15], PanoOcc [14] first generate a compact low-resolution volume and then recover the geometric details via voxel upsampling.

In addition to directly constructing the 3D volume, some methods [11]–[13], [27], [28] seek more efficient dense representations. TPVFormer [13] proposes a Tri-perspective view (TPV) representation, where each TPV plane aggregates image features through deformable attention, and each voxel is modeled as the sum of its projected features onto the three planes. To further enhance deployment friendliness, FlashOcc [11] compresses the 3D scene into a BEV representation and adopts a channel-to-height decoding strategy to directly infer voxel-level occupancy from it.

2) *Sparse Scene Representation*: Given the spatial sparsity of driving scenarios, sparse scene representation [16]–[21], [29], [30] focuses on modeling non-free areas, thereby avoiding redundant computations for large free spaces. SparseOcc [16] proposes a sparse voxel decoder that progressively reconstructs sparse 3D voxel representations of occupied regions through multi-stage sparsification and refinement. However, the sparsification process heavily relies on the accurate estimation of voxel occupancy scores. OPUS [17] predicts the locations and semantic classes of occupied points with a set of learnable queries, eliminating the need for explicit space modeling or complex sparsification procedures. Recent advances adopt parametric geometric primitives as the fundamental units for scene representation. GaussianFormer [18] and GaussianFormer-2 [19] utilize a set of 3D semantic gaussians to sparsely describe a 3D scene, where each gaussian is responsible for modeling a flexible region of interest. However, the inherent ellipsoidal shape priors limit their ability to model diverse structures. Therefore, QuadricFormer [21] further proposes the 3D semantic superquadric representation, which can efficiently represent complex structures with fewer primitives due to the stronger geometric expressiveness of superquadrics.

B. Camera-based Temporal Modeling

Camera-based temporal modeling aims to exploit historical observations to improve spatial understanding and temporal consistency in 3D perception. Existing methods can be broadly categorized into view-centric and object-centric temporal modeling paradigms.

The view-centric paradigm extracts historical information from structured scene representations across frames, such as perspective view (PV), bird's-eye-view (BEV), or 3D volume representations. Specifically, PV-based methods [4], [5], [16], [17], [31] typically perform temporal modeling by interacting multi-frame PV features with object queries. For example, PETRv2 [4] utilizes 3D position embedding to transform multi-frame, multi-view 2D features into 3D position-aware features, and then object queries interact with these features using global cross-attention. To improve the interaction efficiency, SparseBEV [5], Sparse4D [31], SparseOcc [16], OPUS [17] adopt adaptive sparse sampling and aggregation. In parallel, BEV/volume-based methods [2], [14], [32]–[41] focus on the fusion of multi-frame BEV/volume features. SOLO-Fusion [32], PanoOcc [14], GSD-Occ [33] and ALOcc [34] align historical features to the current frame based on ego-motion, and then fuse them with current features via feature

concatenation. BEVFormer [2] and ViewFormer [36] utilize temporal self-attention to extract temporal information from history BEV features.

The object-centric paradigm propagates temporal information with sparse queries. Representative methods such as StreamPETR [42], Sparse4Dv2 [43], Sparse4Dv3 [44] propagate temporal information through query propagation and temporal cross-attention between current and historical queries.

III. METHOD

A. Preliminaries: 3D Semantic Superquadric Representation

The 3D semantic superquadric representation utilizes a set of general posed superquadric primitives to describe a 3D scene:

$$\mathcal{S} = \{\mathbf{S}^i\}_{i=1}^M = \{(\mathbf{m}^i, \mathbf{r}^i, \mathbf{s}^i, \epsilon^i, \sigma^i, \mathbf{c}^i)\}_{i=1}^M, \quad (1)$$

where the center $\mathbf{m} = (m_x, m_y, m_z)^T$ and rotation $\mathbf{r} \in \mathbb{R}^4$ specify the pose of the superellipsoid. $\mathbf{s} = (s_x, s_y, s_z)^T$ determines the scaling factors along the three axes, while the squareness parameter $\epsilon = (\epsilon_1, \epsilon_2)^T$ controls the squareness of the shape. Opacity σ and semantic probability \mathbf{c} are equipped to incorporate semantic information.

QuadricFormer [21] interprets each superquadric as a continuous occupancy field that describes the occupancy probability in its local neighborhood rather than a hard surface boundary. Specifically, for a 3D point \mathbf{p} , the probability of it being occupied by the superquadric \mathbf{S} is defined as:

$$p_o(\mathbf{p}; \mathbf{S}) = \exp\left(-\lambda\left(\left(\left(\frac{|x'|}{s_x}\right)^{\frac{2}{\epsilon_2}} + \left(\frac{|y'|}{s_y}\right)^{\frac{2}{\epsilon_2}}\right)^{\frac{\epsilon_2}{\epsilon_1}} + \left(\frac{|z'|}{s_z}\right)^{\frac{2}{\epsilon_1}}\right)\right), \quad (2)$$

where λ is a temperature parameter controlling the decay rate of the occupancy probability, and $\mathbf{p}' = (x', y', z')^T$ denotes the coordinates of point \mathbf{p} in the local coordinate system of the superquadric. The local coordinates are obtained via a rotation and translation:

$$\mathbf{p}' = \mathbf{R}^T(\mathbf{p} - \mathbf{m}), \quad (3)$$

where $\mathbf{R} \in SO(3)$ is the rotation matrix derived from the rotation \mathbf{r} . Assuming that the occupancy events associated with different superquadrics at point \mathbf{p} are mutually independent, the overall occupancy probability is derived as the complement of the joint non-occupancy probability:

$$p_o(\mathbf{p}) = 1 - \prod_{i=1}^M (1 - p_o(\mathbf{p}; \mathbf{S}^i)). \quad (4)$$

The semantic prediction of the point \mathbf{p} is formulated as a weighted aggregation of the semantic predictions of all contributing superquadrics:

$$p_s(\mathbf{p}) = \frac{\sum_{i=1}^M p_o(\mathbf{p}; \mathbf{S}^i) \sigma^i \mathbf{c}^i}{\sum_{j=1}^M p_o(\mathbf{p}; \mathbf{S}^j) \sigma^j}. \quad (5)$$

Finally, the semantic occupancy prediction is generated as:

$$o(\mathbf{p}) = [p_o(\mathbf{p}) \cdot p_s(\mathbf{p}); 1 - p_o(\mathbf{p})], \quad (6)$$

where $p_o(\mathbf{p})$ weights the semantic prediction and $1 - p_o(\mathbf{p})$ corresponds to the probability of the empty class.

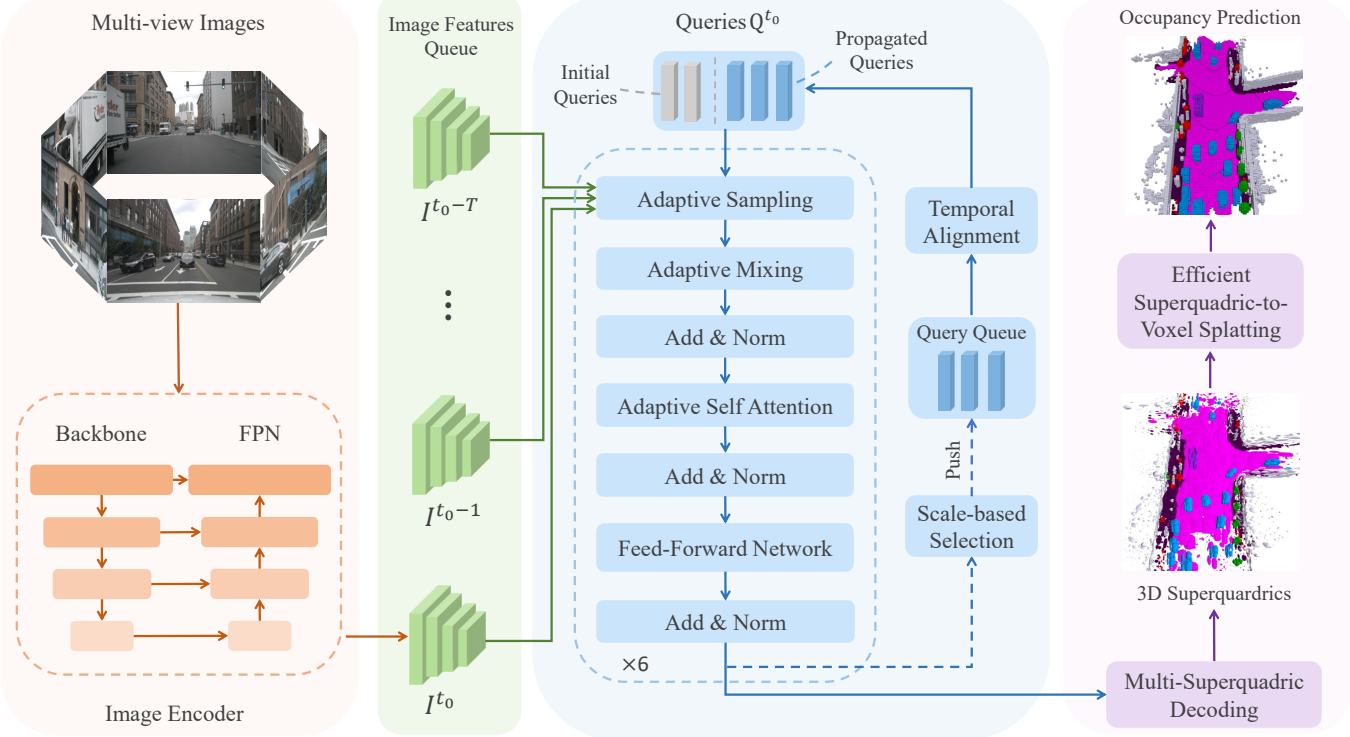


Fig. 2. Framework of SuperOcc. Given multi-view image sequences, SuperOcc constructs a superquadric-based sparse scene representation for 3D occupancy prediction. To achieve comprehensive temporal modeling, the framework extracts fine-grained spatio-temporal context through the interaction of sparse queries with multi-frame image features, while efficiently exploiting informative historical priors via query propagation. Furthermore, each updated query is decoded into a set of semantic superquadrics through a multi-superquadric decoding strategy. Finally, voxel-level occupancy prediction is generated through an efficient superquadric-to-voxel splatting process.

B. Overall framework

As illustrated in Fig. 2, SuperOcc follows an encoder-decoder architecture. The image encoder comprises a backbone (e.g., ResNet50 [45]) and a neck (e.g., FPN [46]). Given multi-view images at time t as input, the image encoder extracts multi-scale features denoted as $I^t = \{I^{t,v,l} \in \mathbb{R}^{C \times H_l \times W_l} | 1 \leq l \leq L, 1 \leq v \leq V\}$, where V and L represent the number of camera views and feature scales, respectively. H_l and W_l denote the feature resolution at the l -th feature scale. To leverage temporal information, the image features from the most recent T frames are maintained in a memory queue, denoted as $\mathcal{I} = \{I^t\}_{t=t_0-T}^{t_0}$.

Subsequently, we initialize a set of queries $Q = \{\mathbf{q}^i \in \mathbb{R}^C\}_{i=1}^{N_q}$ and a corresponding set of 3D reference points $P_{ref} = \{\mathbf{p}_{ref}^i \in \mathbb{R}^3\}_{i=1}^{N_q}$ in the decoder. To achieve comprehensive temporal modeling, SuperOcc integrates view-centric and object-centric paradigms within a unified framework. Specifically, the view-centric path adaptively samples and aggregates multi-frame image features from a memory queue to capture detailed spatio-temporal cues guided by the queries. Simultaneously, the object-centric path propagates historical queries to the subsequent frame, enabling the preservation and reuse of object-level semantic and spatial priors across frames. These queries then interact globally through adaptive self-attention [5]. Finally, the updated query features are decoded into geometric parameters and semantic logits for a set of superquadrics, which are then transformed into voxel-level

occupancy prediction via an efficient superquadric-to-voxel splatting scheme.

C. Cohesive Temporal Modeling

1) *View-centric Temporal Modeling*: The view-centric path is designed to extract fine-grained temporal cues from historical observation sequences. By leveraging geometric constraints and ego-motion compensation, it adaptively samples spatio-temporal features from the image feature queue \mathcal{I} and aggregates them into a unified 4D representation.

Specifically, for each query \mathbf{q} and its corresponding 3D reference point $\mathbf{p}_{ref} = (x, y, z)$, we first utilize a linear layer to predict a set of sampling offsets:

$$\{(\Delta x^i, \Delta y^i, \Delta z^i)\}_{i=1}^{N_s} = \text{Linear}(\mathbf{q}). \quad (7)$$

These offsets are subsequently added to the reference point to generate a set of 3D sampling points:

$$\mathcal{P}_s = \{\mathbf{p}^i = (x + \Delta x^i, y + \Delta y^i, z + \Delta z^i)\}_{i=1}^{N_s}. \quad (8)$$

This sampling strategy allows queries to adaptively adjust the receptive field to capture more discriminative features.

To sample features from any time t within the memory queue \mathcal{I} , we project each sampling point onto the hit camera views based on ego-motion compensation and camera param-

eters. The sampled feature $f^{t,i}$ for the i -th point at time t is extracted via bilinear interpolation as follows:

$$f^{t,i} = \frac{1}{|V_{hit}|} \sum_{v \in V_{hit}} \sum_{l=1}^L w^{i,l} \cdot \mathcal{BS}(I^{t,v,l}, \pi_v(T_{t_0 \rightarrow t} p^i)), \quad (9)$$

where V_{hit} is the set of hit camera views, $T_{t_0 \rightarrow t} \in \mathbb{R}^{4 \times 4}$ denotes the ego-motion transformation matrix that transforms the 3D coordinates from the current coordinate frame at time t_0 to the target frame at time t . $\pi_v(\cdot)$ denotes the projection function onto the v -th image plane, and $\mathcal{BS}(\cdot)$ denotes the bilinear sampling function. The term $w^{i,l}$ represents the weight predicted by the query for the i -th sampling point on the l -th feature scale.

To aggregate the spatio-temporal evidence from different timestamps and sampling points, we organize the extracted features into $f_{st} \in \mathbb{R}^{M \times C}$, where $M = T \times N_s$ represents the total number of sampled features across T frames. Then, adaptive mixing [5], [17] is employed to transform f_{st} along the channel and spatial dimensions under the guidance of the query. The resulting features are then aggregated into the query feature to produce an updated representation.

2) *Object-centric Temporal Modeling*: Sparse queries compactly encode the geometric and semantic information of the scene. Given the inherent temporal continuity of the evolution of driving scenarios, sparse query representations in adjacent frames exhibit strong correlation. Based on this observation, object-centric temporal modeling propagates these queries across frames, enabling efficient exploitation of informative historical spatial and semantic priors.

Specifically, we maintain a memory queue of size N_p to store selected queries from the previous frame. Since these selected queries are expected to predominantly cover foreground regions, an effective selection strategy is crucial. In our formulation, the occupancy field associated with each query is determined by its predicted superquadric parameters. In particular, the scale vector $\mathbf{s} = (s_x, s_y, s_z)^T$ controls the spatial extent of the field and thus reflects the geometric contribution of the query to the foreground. A larger scale typically indicates a more substantial contribution. Thus, we define the foreground score ζ of each query as the maximum scale among its K predicted superquadrics:

$$\zeta = \max_{k \in \{1, \dots, K\}} (\max(s_x^k, s_y^k, s_z^k)). \quad (10)$$

At each frame, the top- N_p queries with the highest foreground scores and their reference points P_p are pushed into a memory queue. After temporal alignment, they are propagated to the next frame. To alleviate potential spatial redundancy between propagated queries and newly initialized ones, we discard initialized queries whose reference points lie within a distance threshold τ (e.g., $\tau = 1.0$ m) of any propagated reference point. Then, the query set is complemented by stochastically sampling $N_q - N_p$ candidates from the residual initialization queries to maintain a constant budget N_q . This ensures that the hybrid queries provide both stable temporal priors for persistent objects and sufficient exploratory coverage for newborn objects.

D. Multi-Superquadric Decoding Strategy

Existing superquadric-based methods [21], [22] typically decode each query into a single superquadric primitive. However, a single superquadric struggles to accurately represent irregular local geometry in real-world driving scenes, which forces the model to rely on high-density queries to achieve adequate geometric fidelity. To amplify the geometric expressiveness of the model without compromising the sparsity of the query representation, we propose the multi-superquadric decoding strategy. Under this strategy, each query \mathbf{q} predicts a local superquadric cluster \mathcal{S}_{local} composed of K superquadrics:

$$\mathcal{S}_{local} = \{\mathbf{S}^k\}_{k=1}^K = \{(\mathbf{p}_{ref} + \mathbf{o}^k, \mathbf{r}^k, \mathbf{s}^k, \epsilon^k, \sigma^k, \mathbf{c})\}_{k=1}^K, \quad (11)$$

where \mathbf{o}^k represents the predicted offset of the k -th superquadric center relative to the reference point \mathbf{p}_{ref} . All geometric parameters together with the opacity are generated by a regression head ϕ_{reg} :

$$\{(\mathbf{o}^k, \mathbf{r}^k, \mathbf{s}^k, \epsilon^k, \sigma^k)\}_{k=1}^K = \phi_{reg}(\mathbf{q}). \quad (12)$$

The semantic logits \mathbf{c} are shared across the cluster and predicted by a classification head ϕ_{cls} :

$$\mathbf{c} = \phi_{cls}(\mathbf{q}). \quad (13)$$

Furthermore, we employ a coarse-to-fine prediction mechanism to guide the decoder in smoothly transitioning from coarse structural approximation to fine-grained geometric refinement. Specifically, as the decoding depth increases, the number of superquadrics K predicted by each query is progressively increased.

E. Efficient Superquadric-to-Voxel Splatting

The superquadric-to-voxel splatting aims to transform the predicted superquadrics into a volumetric semantic occupancy representation via a local aggregation operator. Considering the locality of the superquadric distribution, Quadric-Former [21] first estimates the splatting radius based on the superquadric scale \mathbf{s} , and then determines the contributing superquadrics for each voxel through a matching and sorting procedure. During the splatting phase, a dedicated thread is assigned to each voxel to compute its occupancy probability and semantic logits.

However, this voxel-level binning strategy suffers from two major bottlenecks: 1) The massive number of matching pairs formed between superquadrics and voxels significantly escalates the computational complexity of the sorting process. 2) Neighboring voxels typically interact with highly similar sets of superquadrics. However, their corresponding threads necessitate redundant global memory transactions, leading to substantial memory bandwidth overhead.

To address these issues, inspired by the tile-based rasterization in gaussian splatting [47], we partition the entire 3D space into cubic tiles of size $4 \times 4 \times 4$ voxels and perform binning operation at the tile level. This fundamentally reduces the population of matching pairs, thereby alleviating the sorting complexity. During the splatting stage, each tile is processed by a CUDA thread block, and each thread within the block

still handles one voxel. Crucially, all superquadrics associated with a tile are coalesced and loaded into shared memory for collective reuse by all threads in the block. This mechanism drastically suppresses global memory traffic and significantly enhances overall computational throughput.

IV. EXPERIMENTS

A. Datasets and Evaluation Metric

nuScenes [48] is a large-scale autonomous driving dataset that provides multi-sensor data collected from six cameras, one LiDAR, and five radars. It consists of 1,000 driving sequences, which are divided into 700 for training, 150 for validation, and 150 for testing. Each sequence lasts approximately 20 seconds, with a keyframe sampled every 0.5 seconds for annotation. The Occ3D [48] and SurroundOcc [9] benchmarks provide dense semantic occupancy annotations for the nuScenes dataset. The occupancy annotations in Occ3D span [-40m, 40m] along the X and Y axes, [-1m, 5.4m] along the Z axis, with a resolution of $200 \times 200 \times 16$. It contains 17 semantic classes and one empty class. In comparison, SurroundOcc extends the spatial range to [-50m, 50m] along the X and Y axes and [-5m, 3m] along the Z axis, while maintaining the same $200 \times 200 \times 16$ resolution. Each voxel is labeled as one of 18 classes, including 16 semantic classes, one empty class, and one unknown class.

We adopt two evaluation metrics for SurroundOcc: the Intersection-over-Union (IoU) of occupied voxels ignoring semantic classes, and the mean IoU (mIoU) across all semantic classes. They are defined as:

$$\text{IoU} = \frac{TP_{\neq c_0}}{TP_{\neq c_0} + FP_{\neq c_0} + FN_{\neq c_0}}, \quad (14)$$

$$\text{mIoU} = \frac{1}{C'} \sum_{i \in C'} \frac{TP_i}{TP_i + FP_i + FN_i}, \quad (15)$$

where C' , c_0 , TP , FP , FN denote the nonempty classes, the empty class, the number of true positive, false positive and false negative predictions, respectively. For Occ3D, we report the mIoU and the Ray-based IoU (RayIoU) [16]. RayIoU is computed at three distance thresholds of 1, 2, and 4 meters, denoted as RayIoU_{1m} , RayIoU_{2m} , and RayIoU_{4m} . The final RayIoU score is obtained by averaging these three values.

B. Implementation Details

Following previous works [16], [17], the input images are resized to 704×256 . We adopt a ResNet-50 [45] backbone with a FPN [46] neck as the image encoder, where the backbone is initialized by nuImages [48] pre-training. To explore the trade-off between efficiency and performance, we scale our model into four variants, namely SuperOcc-T, SuperOcc-S, SuperOcc-M, and SuperOcc-L. These variants employ 0.6K, 1.2K, 2.4K, and 3.6K queries, respectively. The specific configurations for each variant are detailed in Tab. I.

During training, we employ the AdamW [49] optimizer with a weight decay of 1×10^{-2} and a batch size of 8. The learning rate is initialized at 2×10^{-4} and decayed with a cosine annealing schedule. For comparison with SOTA methods, the

TABLE I
CONFIGURATIONS FOR DIFFERENT VARIANTS

Model	N_q	N_s	N_p	superquadric number				
				K1	K2	K3	K4	K5
SuperOcc-T	600	4	500	2	2	4	4	8
SuperOcc-S	1200	2	1000	2	2	4	4	8
SuperOcc-M	2400	2	2000	1	1	2	2	4
SuperOcc-L	3600	2	3000	1	1	2	2	4

models are trained for 48 epochs on Occ3D [6] and 24 epochs on SurroundOcc [9], respectively. For ablation studies, all experiments are conducted using the SuperOcc-T variant and trained for 24 epoch on Occ3D. FPS is evaluated on a single NVIDIA RTX 4090 GPU using the PyTorch FP32 backend with a batch size of 1.

C. Main Results

1) *Comparasion on Occ3D*: We compare SuperOcc with recent occupancy prediction methods on the Occ3D [6] benchmark. As reported in Tab. II, SuperOcc establishes new SOTA performance while achieving a superior trade-off between prediction accuracy and inference efficiency.

Compared with the representative sparse predictor OPUS [17], SuperOcc-T achieves 42.5% RayIoU and 30.3 FPS, surpassing OPUS-L in prediction accuracy and outperforming OPUS-T in inference speed. By scaling up the model, SuperOcc-S/M/L achieve further performance improvements. In particular, SuperOcc-L reaches 38.1% mIoU and 44.0% RayIoU, outperforming the previous SOTA ALOcc-3D [34] by 0.3% RayIoU while maintaining nearly twice the inference throughput of ALOcc-3D (12.7 vs. 6.0 FPS). Moreover, these results demonstrate the strong scalability of SuperOcc: by simply adjusting parameters such as the number of queries, the model achieves a flexible and controllable trade-off between accuracy and efficiency. This enables SuperOcc to meet diverse real-world requirements for both real-time performance and high prediction accuracy.

2) *Comparasion on SurroundOcc*: In Tab. III, we present a comprehensive comparison with other SOTA 3D semantic occupancy prediction methods on the SurroundOcc benchmark. Our SuperOcc family consistently demonstrates a commanding performance lead over existing approaches.

Specifically, compared with the advanced temporal-aware predictor GaussianWorld [20], SuperOcc achieves higher IoU and mIoU even under a weaker setting (ResNet-50 [45] vs. ResNet101-DCN [45], and input resolution 256×704 vs. 900×1600). Furthermore, compared with the recent superquadric-based predictor QuadricFormer [21], our method also exhibits significant performance margins. In particular, SuperOcc-T outperforms QuadricFormer by 3.69% IoU and 2.36% mIoU, while providing substantially higher inference throughput. These results collectively establish SuperOcc as a more effective and efficient superquadric-based occupancy prediction framework.

TABLE II
OCCUPANCY PREDICTION PERFORMANCE ON OCC3D [6] BENCHMARK "8F" AND "16F" DENOTE MODELS FUSING TEMPORAL INFORMATION FROM 8 OR 16 FRAMES, RESPECTIVELY. FPS RESULTS ARE MEASURED ON A SINGLE RTX 4090 GPU

Methods	Backbone	Image Size	Epoch	Vis.Mask	mIoU	RayIoU _{1m}	RayIoU _{2m}	RayIoU _{4m}	RayIoU	FPS
RenderOcc [50]	Swin-B	1408 × 512	12	✓	24.5	13.4	19.6	25.5	19.5	-
BEVFormer [2]	R101	1600 × 900	24	✓	39.3	26.1	32.9	38.0	32.4	4.4
BEVDer-Occ (2f) [1]	R50	704 × 256	90	✓	36.1	23.6	30.0	35.1	29.6	9.0
BEVDer-Occ (8f) [1]	R50	704 × 384	90	✓	39.3	26.6	33.1	38.2	32.6	5.6
SparseOcc (8f) [16]	R50	704 × 256	24	-	30.9	28.0	34.7	39.4	34.0	20.9
SparseOcc (16f) [16]	R50	704 × 256	24	-	30.6	29.1	35.8	40.3	35.1	15.9
P-FlashOcc-Tiny (1f) [12]	R50	704 × 256	24	-	29.1	29.1	35.7	39.7	34.8	41.9
P-FlashOcc (1f) [12]	R50	704 × 256	24	-	29.4	29.4	36.0	40.1	35.2	33.8
P-FlashOcc (2f) [12]	R50	704 × 256	24	-	30.3	31.2	37.6	41.5	36.8	29.8
P-FlashOcc (8f) [12]	R50	704 × 256	24	-	31.6	32.8	39.3	43.4	38.5	26.8
GSD-Occ (16f) [33]	R50	704 × 256	24	-	31.8	-	-	-	38.9	-
FB-Occ (16f) [8]	R50	704 × 256	24	-	31.1	33.0	40.0	44.0	39.0	10.3
OPUS-T (8f) [17]	R50	704 × 256	100	-	33.2	31.7	39.2	44.3	38.4	25.1
OPUS-S (8f) [17]	R50	704 × 256	100	-	34.2	32.6	39.9	44.7	39.1	24.5
OPUS-M (8f) [17]	R50	704 × 256	100	-	35.6	33.7	41.1	46.0	40.3	17.8
OPUS-L (8f) [17]	R50	704 × 256	100	-	36.2	34.7	42.1	46.7	41.2	8.6
STCOcc (8f) [29]	R50	704 × 256	36	-	-	36.2	42.7	46.4	41.7	-
ALOcc-2D-mini (16f) [34]	R50	704 × 256	54	-	33.4	32.9	40.1	44.8	39.3	30.5
ALOcc-2D (16f) [34]	R50	704 × 256	54	-	37.4	37.1	43.8	48.2	43.0	8.2
ALOcc-3D (16f) [34]	R50	704 × 256	54	-	38.0	37.8	44.7	48.8	43.7	6.0
SuperOcc-T (8f)	R50	704 × 256	48	-	36.1	36.6	43.4	47.6	42.5	30.3
SuperOcc-S (8f)	R50	704 × 256	48	-	36.9	37.2	43.7	48.0	43.0	28.2
SuperOcc-M (8f)	R50	704 × 256	48	-	37.4	37.8	44.4	48.6	43.6	18.8
SuperOcc-L (8f)	R50	704 × 256	48	-	38.1	38.3	44.8	48.9	44.0	12.7

TABLE III
3D SEMANTIC OCCUPANCY PREDICTION RESULTS ON SURROUNDOCC [9] BENCHMARK. * MEANS SUPERVISED BY DENSE OCCUPANCY ANNOTATIONS AS OPPOSED TO ORIGINAL LiDAR SEGMENTATION LABELS. FPS RESULTS ARE MEASURED ON A SINGLE RTX 4090 GPU

Method	IoU	mIoU	barrier	bicycle	bus	car	const. veh.	motorcycle	pedestrian	traffic cone	trailer	truck	drive. suf.	other flat	sidewalk	terrain	manmade	vegetation	FPS
			■	■	■	■	■	■	■	■	■	■	■	■	■	■	■		
MonoScene [23]	23.96	7.31	4.03	0.35	8.00	8.04	2.90	0.28	1.16	0.67	4.01	4.35	27.72	5.20	15.13	11.29	9.03	14.86	-
Atlas [51]	28.66	15.00	10.64	5.68	19.66	24.94	8.90	8.84	6.47	3.28	10.42	16.21	34.86	15.46	21.89	20.95	11.21	20.54	-
BEVFormer [2]	30.50	16.75	14.22	6.58	23.46	28.28	8.66	10.77	6.64	4.05	11.20	17.78	37.28	18.00	22.88	22.17	13.80	22.21	3.3
TPVFormer [13]	11.51	11.66	16.14	7.17	22.63	17.13	8.83	11.39	10.46	8.23	9.43	17.02	8.07	13.64	13.85	10.34	4.90	7.37	2.9
TPVFormer* [13]	30.86	17.10	15.96	5.31	23.86	27.32	9.79	8.74	7.09	5.20	10.97	19.22	38.87	21.25	24.26	23.15	11.73	20.81	2.9
OccFormer [10]	31.39	19.03	18.65	10.41	23.92	30.29	10.31	14.19	13.59	10.13	12.49	20.77	38.78	19.79	24.19	22.21	13.48	21.35	-
SurroundOcc [9]	31.49	20.30	20.59	11.68	28.06	30.86	10.70	15.14	14.09	12.06	14.38	22.26	37.29	23.70	24.49	22.77	14.89	21.86	3.3
GaussianFormer [18]	29.83	19.10	19.52	11.26	26.11	29.78	10.47	13.83	12.58	8.67	12.74	21.57	39.63	23.28	24.46	22.99	9.59	19.12	2.7
GaussianFormer-2 [19]	30.56	20.02	20.15	12.99	27.61	30.23	11.19	15.31	12.64	9.63	13.31	22.26	39.68	23.47	25.62	23.20	12.25	20.73	2.8
QuadricFormer [21]	31.22	20.12	19.58	13.11	27.27	29.64	11.25	16.26	12.65	9.15	12.51	21.24	40.20	24.34	25.69	24.24	12.95	21.86	-
GaussianWorld [20]	33.40	22.13	21.38	14.12	27.71	31.84	13.66	17.43	13.66	11.46	15.09	23.94	42.98	24.86	28.84	26.74	15.69	24.74	4.4
SuperOcc-T	34.91	22.48	21.35	11.90	28.35	32.12	15.46	15.84	13.20	11.83	11.87	23.71	47.30	29.19	30.29	28.22	13.23	25.75	30.3
SuperOcc-S	35.63	23.15	21.96	12.14	28.46	32.86	16.98	16.62	13.60	13.06	12.40	24.52	47.16	29.07	30.81	28.46	14.90	26.87	28.2
SuperOcc-M	36.99	23.95	23.73	12.07	28.46	33.13	17.42	17.68	14.62	14.20	12.87	25.27	47.84	29.33	31.58	29.15	17.28	28.55	18.8
SuperOcc-L	38.13	24.55	23.92	12.43	29.77	33.62	17.36	17.74	14.95	14.79	13.42	26.25	48.22	29.22	32.16	30.20	18.67	30.04	12.7

TABLE IV
ABLATION OF DIFFERENT COMPONENTS IN SUPER OCC.
MDS: MULTI-SUPERQUADRIC DECODING; CTM: COHESIVE TEMPORAL MODELING

MSD	CTM	mIoU	RayIoU	RayIoU _{1m, 2m, 4m}	FPS
✓		27.9	33.3	26.9 34.0 39.0	33.0
✓	✓	29.1	34.9	28.6 35.6 40.5	31.7
✓	✓	33.8	39.5	33.4 40.4 44.8	31.2
✓	✓	35.4	41.2	35.0 41.9 46.5	30.3

D. Ablation Studies

1) *Component analysis:* We conduct a comprehensive ablation study in Tab. IV to quantify the individual contribution

of each proposed component in the SuperOcc framework.

The baseline relies solely on single-frame image inputs and single-superquadric decoding. Starting from the baseline, incorporating the proposed multi-superquadric decoding (MSD) strategy yields an improvement of 1.2% mIoU and 1.6% RayIoU, with only a marginal increase in inference latency. This indicates that MSD effectively enhances geometric expressiveness while completely preserving the query sparsity. When equipping the baseline with the cohesive temporal modeling (CTM) mechanism, we observe a substantial performance gain of 5.9% mIoU and 6.2% RayIoU. This remarkable performance leap underscores the effectiveness and necessity

TABLE V
ABLATION OF MULTI-SUPERQUADRIC DECODING

K1-K6	mIoU	RayIoU	RayIoU _{1m, 2m, 4m}		
[1, 1, 1, 1, 1, 1]	27.9	33.3	26.9	34.0	39.0
[2, 2, 2, 2, 2, 2]	28.4	33.9	27.4	34.6	39.6
[4, 4, 4, 4, 4, 4]	28.8	34.6	28.4	35.3	40.2
[8, 8, 8, 8, 8, 8]	28.8	34.9	28.7	35.6	40.4
[16, 16, 16, 16, 16, 16]	28.7	34.5	28.2	35.1	40.0
[2, 2, 4, 4, 8, 8]	29.1	34.9	28.6	35.6	40.5

TABLE VI
ABLATION OF COHESIVE TEMPORAL MODELING

View-centric	Object-centric	mIoU	RayIoU	RayIoU _{1m, 2m, 4m}		
✓	✓	29.1	34.9	28.6	35.6	40.5
		34.5	39.6	33.6	40.4	44.9
	✓	31.6	37.6	31.3	38.3	43.2
✓	✓	35.4	41.2	35.0	41.9	46.5

of our CTM mechanism. By combining all components, SuperOcc achieves a significant overall improvement of 7.5% mIoU and 7.9% RayIoU over the baseline. Although this configuration incurs a moderate reduction in FPS, it maintains a real-time inference speed of 30.3 FPS, offering a favorable trade-off between accuracy and efficiency.

2) *Effect of Multi-Superquadric Decoding*: The number of superquadrics predicted per query is a critical factor in our MSD strategy. As summarized in Tab. V, we conduct an ablation study to analyze its impact.

The first five rows report the performance when varying the number of predicted superquadrics without the coarse-to-fine mechanism. We observe that occupancy prediction performance improves steadily with the number of superquadrics, and begins to saturate at $K = 8$. This demonstrates that while MSD effectively improves geometric expressiveness, an optimal number of primitives is essential to balance representational capacity and optimization stability, with $K = 8$ providing the best trade-off in our settings.

In the final row, we incorporate the coarse-to-fine strategy, where the number of predicted superquadrics is progressively increased across decoding stages. This configuration further boosts performance, achieving the highest mIoU of 29.1% and RayIoU of 34.9%. This suggests that the coarse-to-fine strategy facilitates the learning process by allowing the network to progressively optimize geometric representations from coarse structures to fine details.

3) *Effect of Cohesive Temporal Modeling*: To explore the impact of different temporal modeling strategies, we conduct a comprehensive ablation study as shown in Tab. VI. Without temporal modeling, the baseline achieves limited performance, reflecting the inherent difficulty of accurately predicting 3D occupancy from single-frame inputs. It can be observed that incorporating view-centric temporal modeling significantly boosts mIoU and RayIoU by 5.4% and 4.7%, respectively. This demonstrates that the rich spatio-temporal context provided by historical observations is crucial for inferring the current occupancy. Meanwhile, object-centric temporal modeling also yields noticeable gains (+2.5% mIoU and +2.7% RayIoU),

TABLE VII
ABLATION STUDY ON DIFFERENT QUERY SELECTION STRATEGIES IN OBJECT-CENTRIC TEMPORAL MODELING

Selection Strategy	mIoU	RayIoU	RayIoU _{1m, 2m, 4m}		
No selection	25.3	31.1	24.9	31.7	36.6
Semantic logit-based	29.5	35.4	29.0	36.1	41.1
Opacity-based	29.3	35.6	29.2	36.2	41.2
Scale-based (ours)	31.6	37.6	31.3	38.3	43.2

TABLE VIII
ABLATION OF THE EFFICIENT SUPERQUADRIC-TO-VOXEL SPLATTING

ESS	Training Phase		Inference Phase		FPS
	Mem (GB)	Time (h)	Mem (GB)	Splatting Latency (ms)	
✓	21.4 17.3 (-19%)	82 20 (-76%)	3.1 2.8 (-9%)	6.2 1.3 (-79%)	25.2 30.3 (+20%)

suggesting that the spatial and semantic priors propagated via historical queries can effectively guide the current decoding process. When view-centric and object-centric temporal modeling are jointly applied, the model achieves the best performance across all evaluation metrics. This result strongly validates the complementarity of the two modeling strategies, demonstrating that their integration is essential for achieving accurate 3D occupancy prediction.

4) *Effect of Scale-based Query Selection*: Table VII investigates various query selection strategies for object-centric temporal modeling. Directly propagating all queries results in a noticeable performance drop, as the propagated queries tend to dominate the optimization process and impede the effective learning of initialization queries. While strategies based on semantic logits or opacity partially mitigate this, they achieve suboptimal performance because neither semantic confidence nor opacity reliably reflects a query's foreground contribution. In contrast, our scale-based selection achieves the best performance. This indicates that scale-based selection is more effective at identifying foreground queries, thereby providing more stable and efficient temporal priors for subsequent frames.

5) *Effect of Efficient Superquadric-to-Voxel Splatting*: To evaluate the impact of the proposed efficient superquadric-to-voxel splatting (ESS), we conduct a comparative analysis as summarized in Tab. VIII. The experimental results demonstrate that ESS significantly reduces computational costs across both the training and inference stages.

In the training phase, the integration of ESS significantly boosts training efficiency. Notably, it achieves a 76% reduction in wall-clock training time (from 82 h to 20 h) while simultaneously lowering the GPU memory footprint by 19% (from 21.4 GB to 17.3 GB). This drastic acceleration demonstrates that our optimized splatting operator effectively alleviates the computational bottlenecks in the superquadric-to-voxel transformation during both forward and backward propagation. In the inference phase, ESS slashes the splatting latency by 79%, from 6.2 ms to 1.3 ms. Consequently, the overall system throughput is increased by 20%, reaching 30.3 FPS. This reduction in computational overhead significantly enhances the deployment potential of our framework.

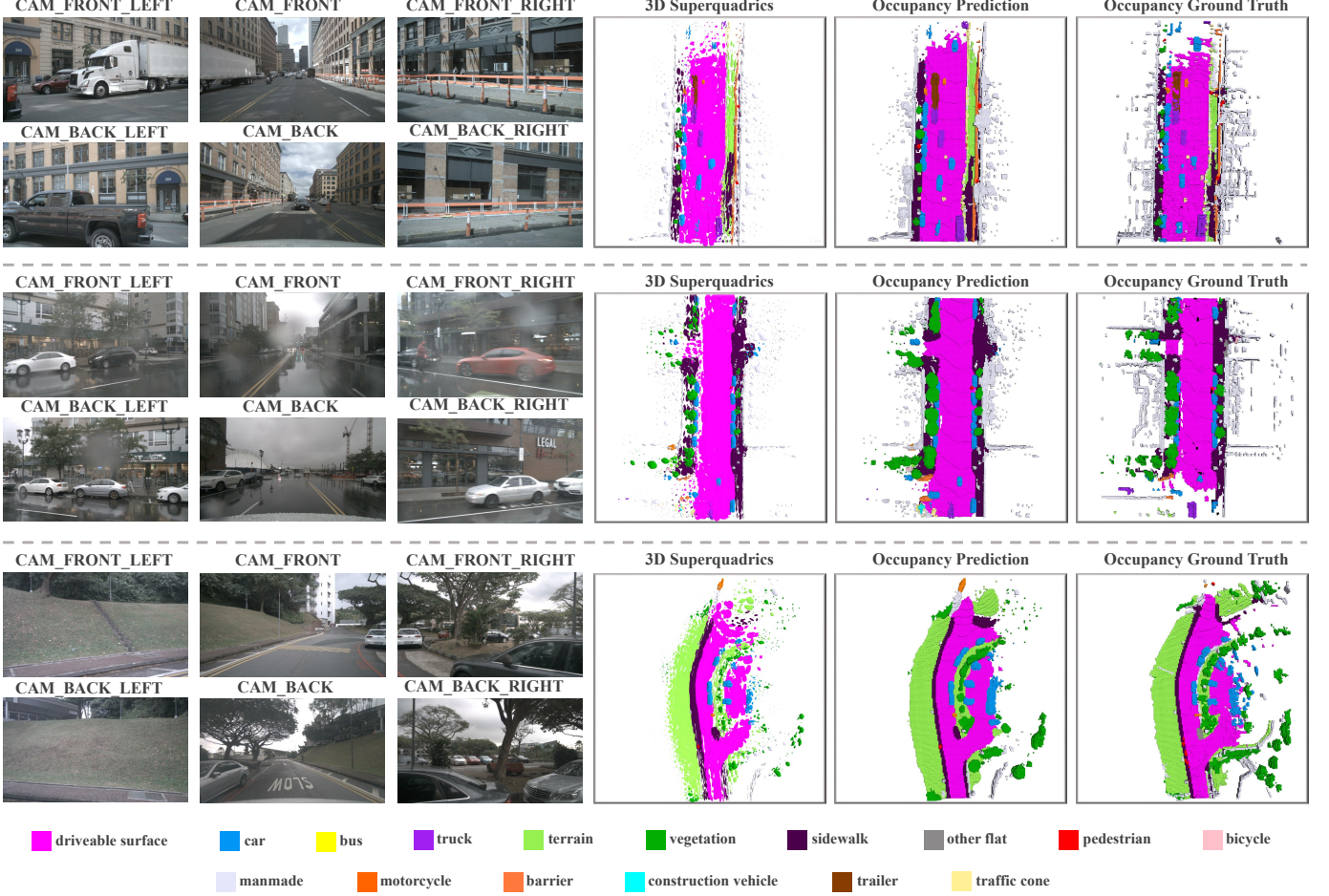


Fig. 3. Qualitative results of SuperOcc on the SurroundOcc [9] benchmark. For each scene, the predicted superquadrics, resulting occupancy prediction, and ground-truth occupancy are shown. Colors indicate semantic categories for both superquadrics and voxels.

E. Qualitative Results

Qualitative prediction results of SuperOcc on the SurroundOcc [9] benchmark are shown in Fig. 3. For each scene, we visualize the predicted superquadrics, the resulting occupancy prediction, and the corresponding ground-truth occupancy. Each superquadric and voxel is color-coded according to its semantic category.

The predicted superquadric primitives effectively model the underlying 3D scene geometry in a compact manner. The occupancy predictions derived from these superquadrics exhibit high fidelity to the ground truth, preserving clear structural boundaries between occupied and free space. These results demonstrate that SuperOcc can accurately reconstruct fine-grained scene geometries, highlighting its effectiveness in complex urban environments.

F. Limitations

Although our proposed method achieves significant progress, several limitations remain to be addressed.

First, SuperOcc is restricted to semantic occupancy prediction and has not yet been extended to panoptic occupancy prediction. Specifically, while it can accurately predict the semantic category of each occupied voxel, it lacks the ability to

distinguish different individual instances within the same category. However, such instance-level discrimination is crucial for fine-grained scene understanding in autonomous driving. Second, SuperOcc primarily relies on ego-motion compensation for temporal alignment, without explicitly modeling the motion of dynamic objects. As a result, historical features sampled for dynamic objects may exhibit spatio-temporal misalignment. Moreover, the temporal propagation of queries may introduce less reliable spatial priors, which can adversely affect the occupancy modeling of dynamic objects.

In future work, we plan to extend SuperOcc to panoptic occupancy prediction by incorporating instance-level representations into the superquadric-based framework. Additionally, we aim to integrate explicit object motion modeling to enhance the spatio-temporal consistency for dynamic objects.

V. CONCLUSION

In this paper, we propose SuperOcc, a novel superquadric-based framework for 3D occupancy prediction. By unifying view-centric and object-centric temporal paradigms, SuperOcc effectively exploits fine-grained spatio-temporal context together with historical priors, enabling accurate predictions in dynamic driving environments. Furthermore, SuperOcc

introduces a multi-superquadric decoding strategy that decodes each query into a cluster of superquadrics. This design significantly bolsters the capacity to model complex scenes while preserving query sparsity. Additionally, we optimize the superquadric-to-voxel splatting operation through a CUDA-friendly implementation, dramatically reducing training overhead and splatting latency. Extensive evaluations on public benchmarks validate the effectiveness and efficiency of SuperOcc, demonstrating its clear advantages over existing occupancy prediction methods. We hope that SuperOcc can provide valuable insights into superquadric-based occupancy prediction for the community.

REFERENCES

- [1] J. Huang, G. Huang, Z. Zhu, Y. Yun, and D. Du, “BEVDet: High-performance multi-camera 3d object detection in bird-eye-view,” 2021, *arXiv:2112.11790*.
- [2] Z. Li, W. Wang, H. Li, E. Xie, C. Sima, T. Lu, Y. Qiao, and J. Dai, “BEVFormer: Learning bird’s-eye-view representation from multi-camera images via spatiotemporal transformers,” in *Proc. Eur. Conf. Comput. Vis.* Cham, Switzerland: Springer, Oct. 2022, pp. 1–18.
- [3] Y. Liu, T. Wang, X. Zhang, and J. Sun, “PETR: Position embedding transformation for multi-view 3d object detection,” in *Proc. Eur. Conf. Comput. Vis.* Cham, Switzerland: Springer, Oct. 2022, pp. 531–548.
- [4] Y. Liu, J. Yan, F. Jia, S. Li, A. Gao, T. Wang, and X. Zhang, “PETRv2: A unified framework for 3d perception from multi-camera images,” in *Proc. IEEE/CVF Int. Conf. Comput. Vis.*, Oct. 2023, pp. 3262–3272.
- [5] H. Liu, Y. Teng, T. Lu, H. Wang, and L. Wang, “SparseBEV: High-performance sparse 3d object detection from multi-camera videos,” in *Proc. IEEE/CVF Int. Conf. Comput. Vis.*, Oct. 2023, pp. 18580–18590.
- [6] X. Tian, T. Jiang, L. Yun, Y. Mao, H. Yang, Y. Wang, Y. Wang, and H. Zhao, “Occ3d: A large-scale 3d occupancy prediction benchmark for autonomous driving,” *Proc. Adv. Neural Inform. Process. Syst.*, vol. 36, pp. 64318–64330, Dec. 2023.
- [7] W. Tong, C. Sima, T. Wang, L. Chen, S. Wu, H. Deng, Y. Gu, L. Lu, P. Luo, D. Lin *et al.*, “Scene as occupancy,” in *Proc. IEEE/CVF Int. Conf. Comput. Vis.*, Oct. 2023, pp. 8406–8415.
- [8] Z. Li, Z. Yu, D. Austin, M. Fang, S. Lan, J. Kautz, and J. M. Alvarez, “FB-OCC: 3d occupancy prediction based on forward-backward view transformation,” 2023, *arXiv:2307.01492*.
- [9] Y. Wei, L. Zhao, W. Zheng, Z. Zhu, J. Zhou, and J. Lu, “Surroundocc: Multi-camera 3d occupancy prediction for autonomous driving,” in *Proc. IEEE/CVF Int. Conf. Comput. Vis.*, Oct. 2023, pp. 21729–21740.
- [10] Y. Zhang, Z. Zhu, and D. Du, “Occformer: Dual-path transformer for vision-based 3d semantic occupancy prediction,” in *Proc. IEEE/CVF Int. Conf. Comput. Vis.*, Oct. 2023, pp. 9433–9443.
- [11] Z. Yu, C. Shu, J. Deng, K. Lu, Z. Liu, J. Yu, D. Yang, H. Li, and Y. Chen, “Flashocc: Fast and memory-efficient occupancy prediction via channel-to-height plugin,” 2023, *arXiv:2311.12058*.
- [12] Z. Yu, C. Shu, Q. Sun, Y. Bian, X. Wei, J. Yu, Z. Liu, D. Yang, H. Li, and Y. Chen, “Panoptic-flashocc: An efficient baseline to marry semantic occupancy with panoptic via instance center,” 2024, *arXiv:2406.10527*.
- [13] Y. Huang, W. Zheng, Y. Zhang, J. Zhou, and J. Lu, “Tri-perspective view for vision-based 3d semantic occupancy prediction,” in *Proc. IEEE/CVF Conf. Comput. Vis. Pattern Recog.*, Jun. 2023, pp. 9223–9232.
- [14] Y. Wang, Y. Chen, X. Liao, L. Fan, and Z. Zhang, “Panoocc: Unified occupancy representation for camera-based 3d panoptic segmentation,” in *Proc. IEEE/CVF Conf. Comput. Vis. Pattern Recog.*, Jun. 2024, pp. 17158–17168.
- [15] Q. Ma, X. Tan, Y. Qu, L. Ma, Z. Zhang, and Y. Xie, “Cotr: Compact occupancy transformer for vision-based 3d occupancy prediction,” in *Proc. IEEE/CVF Conf. Comput. Vis. Pattern Recog.*, Jun. 2024, pp. 19936–19945.
- [16] H. Liu, Y. Chen, H. Wang, Z. Yang, T. Li, J. Zeng, L. Chen, H. Li, and L. Wang, “Fully sparse 3d occupancy prediction,” in *Proc. Eur. Conf. Comput. Vis.* Cham, Switzerland: Springer, Oct. 2024, pp. 54–71.
- [17] J. Wang, Z. Liu, Q. Meng, L. Yan, K. Wang, J. Yang, W. Liu, Q. Hou, and M. Cheng, “Opus: occupancy prediction using a sparse set,” in *Proc. Adv. Neural Inform. Process. Syst.*, vol. 37, Dec. 2024, pp. 119861–119885.
- [18] Y. Huang, W. Zheng, Y. Zhang, J. Zhou, and J. Lu, “Gaussianformer: Scene as gaussians for vision-based 3d semantic occupancy prediction,” in *Proc. Eur. Conf. Comput. Vis.* Cham, Switzerland: Springer, 2024, pp. 376–393.
- [19] Y. Huang, A. Thammatadatrakoon, W. Zheng, Y. Zhang, D. Du, and J. Lu, “Gaussianformer-2: Probabilistic gaussian superposition for efficient 3d occupancy prediction,” in *Proc. IEEE/CVF Conf. Comput. Vis. Pattern Recog.*, Jun. 2025, pp. 27477–27486.
- [20] S. Zuo, W. Zheng, Y. Huang, J. Zhou, and J. Lu, “Gaussianworld: Gaussian world model for streaming 3d occupancy prediction,” in *Proc. IEEE/CVF Conf. Comput. Vis. Pattern Recog.*, Jun. 2025, pp. 6772–6781.
- [21] S. Zuo, W. Zheng, X. Han, L. Yang, Y. Pan, and J. Lu, “Quadricformer: Scene as superquadrics for 3d semantic occupancy prediction,” 2025, *arXiv:2506.10977*.
- [22] S. Hayes, R. Mohandas, T. Brophy, A. Boulch, G. Sistu, and C. Eising, “Superquadricocc: Multi-layer gaussian approximation of superquadrics for real-time self-supervised occupancy estimation,” 2025, *arXiv:2511.17361*.
- [23] A.-Q. Cao and R. De Charette, “Monoscene: Monocular 3d semantic scene completion,” in *Proc. IEEE/CVF Conf. Comput. Vis. Pattern Recog.*, Jun. 2022, pp. 3991–4001.
- [24] Y. Li, Z. Yu, C. Choy, C. Xiao, J. M. Alvarez, S. Fidler, C. Feng, and A. Anandkumar, “Voxformer: Sparse voxel transformer for camera-based 3d semantic scene completion,” in *Proc. IEEE/CVF Conf. Comput. Vis. Pattern Recog.*, Jun. 2023, pp. 9087–9098.
- [25] G. Oh, S. Kim, H. Ko, H.-g. Chi, J. Kim, D. Lee, D. Ji, S. Choi, S. Jang, and S. Kim, “3d occupancy prediction with low-resolution queries via prototype-aware view transformation,” in *Proc. IEEE/CVF Conf. Comput. Vis. Pattern Recog.*, Jun. 2025, pp. 17134–17144.
- [26] J. Kim, C. Kang, D. Lee, S. Choi, and J. W. Choi, “Protoocc: Accurate, efficient 3d occupancy prediction using dual branch encoder-prototype query decoder,” in *Proc. AAAI Conf. Artif. Intell.*, vol. 39, no. 4, Feb. 2025, pp. 4284–4292.
- [27] J. Zhang, Y. Zhang, Q. Liu, and Y. Wang, “Lightweight spatial embedding for vision-based 3d occupancy prediction,” 2024, *arXiv:2412.05976*.
- [28] J. Hou, X. Li, W. Guan, G. Zhang, D. Feng, Y. Du, X. Xue, and J. Pu, “Fastocc: Accelerating 3d occupancy prediction by fusing the 2d bird’s-eye view and perspective view,” May 2024, pp. 16425–16431.
- [29] Z. Liao, P. Wei, S. Chen, H. Wang, and Z. Ren, “Stocc: Sparse spatial-temporal cascade renovation for 3d occupancy and scene flow prediction,” in *Proc. IEEE/CVF Conf. Comput. Vis. Pattern Recog.*, Jun. 2025, pp. 1516–1526.
- [30] Y. Shi, T. Cheng, Q. Zhang, W. Liu, and X. Wang, “Occupancy as set of points,” in *Proc. Eur. Conf. Comput. Vis.* Cham, Switzerland: Springer, Oct. 2024, pp. 72–87.
- [31] X. Lin, T. Lin, Z. Pei, L. Huang, and Z. Su, “Sparse4D: Multi-view 3d object detection with sparse spatial-temporal fusion,” 2022, *arXiv:2211.10581*.
- [32] J. Park, C. Xu, S. Yang, K. Keutzer, K. M. Kitani, M. Tomizuka, and W. Zhan, “Time will tell: New outlooks and a baseline for temporal multi-view 3d object detection,” in *Proc. Int. Conf. Learn. Represent.*, May 2023.
- [33] Y. He, W. Chen, S. Wang, T. Xun, and Y. Tan, “Achieving speed-accuracy balance in vision-based 3d occupancy prediction via geometric-semantic disentanglement,” in *Proc. AAAI Conf. Artif. Intell.*, vol. 39, no. 3, Feb. 2025, pp. 3455–3463.
- [34] D. Chen, J. Fang, W. Han, X. Cheng, J. Yin, C. Xu, F. S. Khan, and J. Shen, “Alocc: Adaptive lifting-based 3d semantic occupancy and cost volume-based flow predictions,” in *Proc. IEEE/CVF Int. Conf. Comput. Vis.*, Oct. 2025, pp. 4156–4166.
- [35] D. Chen, H. Zheng, J. Fang, X. Dong, X. Li, W. Liao, T. He, P. Peng, and J. Shen, “Rethinking temporal fusion with a unified gradient descent view for 3d semantic occupancy prediction,” in *Proc. IEEE/CVF Conf. Comput. Vis. Pattern Recog.*, Jun. 2025, pp. 1505–1515.
- [36] J. Li, X. He, C. Zhou, X. Cheng, Y. Wen, and D. Zhang, “Viewformer: Exploring spatiotemporal modeling for multi-view 3d occupancy perception via view-guided transformers,” in *Proc. Eur. Conf. Comput. Vis.* Cham, Switzerland: Springer, Oct. 2024, pp. 90–106.
- [37] Z. Leng, J. Yang, W. Yi, and B. Zhou, “Occupancy learning with spatiotemporal memory,” in *Proc. IEEE/CVF Int. Conf. Comput. Vis.*, Oct. 2025, pp. 26569–26578.
- [38] Z. Zong, D. Jiang, G. Song, Z. Xue, J. Su, H. Li, and Y. Liu, “Temporal enhanced training of multi-view 3d object detector via historical object prediction,” in *Proc. IEEE/CVF Int. Conf. Comput. Vis.*, Oct. 2023, pp. 3781–3790.

- [39] Z. Xia, Z. Lin, X. Wang, Y. Wang, Y. Xing, S. Qi, N. Dong, and M.-H. Yang, “Henet: Hybrid encoding for end-to-end multi-task 3d perception from multi-view cameras,” in *Proc. Eur. Conf. Comput. Vis.* Cham, Switzerland: Springer, Oct. 2024, pp. 376–392.
- [40] M. Chang, X. Zhang, R. Zhang, Z. Zhao, G. He, and S. Liu, “Recurrentbev: A long-term temporal fusion framework for multi-view 3d detection,” in *Proc. Eur. Conf. Comput. Vis.* Cham, Switzerland: Springer, Oct. 2024, pp. 131–147.
- [41] C. Han, J. Yang, J. Sun, Z. Ge, R. Dong, H. Zhou, W. Mao, Y. Peng, and X. Zhang, “Exploring recurrent long-term temporal fusion for multi-view 3d perception,” *IEEE Rob. Autom. Lett.*, vol. 9, no. 7, pp. 6544–6551, 2024.
- [42] S. Wang, Y. Liu, T. Wang, Y. Li, and X. Zhang, “Exploring object-centric temporal modeling for efficient multi-view 3d object detection,” in *Proc. IEEE/CVF Int. Conf. Comput. Vis.*, Oct. 2023, pp. 3621–3631.
- [43] X. Lin, T. Lin, Z. Pei, L. Huang, and Z. Su, “Sparse4d v2: Recurrent temporal fusion with sparse model,” 2023, *arXiv:2305.14018*.
- [44] X. Lin, Z. Pei, T. Lin, L. Huang, and Z. Su, “Sparse4d v3: Advancing end-to-end 3d detection and tracking,” 2023, *arXiv:2311.11722*.
- [45] K. He, X. Zhang, S. Ren, and J. Sun, “Deep residual learning for image recognition,” in *Proc. IEEE/CVF Conf. Comput. Vis. Pattern Recog.*, Jun. 2016, pp. 770–778.
- [46] T.-Y. Lin, P. Dollár, R. Girshick, K. He, B. Hariharan, and S. Belongie, “Feature pyramid networks for object detection,” in *Proc. IEEE/CVF Conf. Comput. Vis. Pattern Recog.*, Jun. 2017, pp. 2117–2125.
- [47] B. Kerbl, G. Kopanas, T. Leimkühler, and G. Drettakis, “3d gaussian splatting for real-time radiance field rendering,” *ACM Trans. Graph.*, vol. 42, no. 4, pp. 139–1, 2023.
- [48] H. Caesar, V. Bankiti, A. H. Lang, S. Vora, V. E. Lioung, Q. Xu, A. Krishnan, Y. Pan, G. Baldan, and O. Beijbom, “nuScenes: A multimodal dataset for autonomous driving,” in *Proc. IEEE/CVF Conf. Comput. Vis. Pattern Recog.*, Jun. 2020, pp. 11621–11631.
- [49] I. Loshchilov and F. Hutter, “Decoupled weight decay regularization,” 2017, *arXiv:1711.05101*.
- [50] M. Pan, J. Liu, R. Zhang, P. Huang, X. Li, H. Xie, B. Wang, L. Liu, and S. Zhang, “Renderocc: Vision-centric 3d occupancy prediction with 2d rendering supervision,” May 2024, pp. 12404–12411.
- [51] Z. Murez, T. Van As, J. Bartolozzi, A. Sinha, V. Badrinarayanan, and A. Rabinovich, “Atlas: End-to-end 3d scene reconstruction from posed images,” in *Proc. Eur. Conf. Comput. Vis.* Cham, Switzerland: Springer, Oct. 2020, pp. 414–431.